

# Hamiltonian engineering for robust quantum state transfer and qubit readout in cavity QED

Félix Beaudoin<sup>1</sup>, Alexandre Blais<sup>2,3</sup>, W. A. Coish<sup>1,3</sup>

<sup>1</sup> Department of Physics, McGill University, Montréal, Québec H3A 2T8, Canada

<sup>2</sup> Département de physique, Université de Sherbrooke, 2500 boulevard de l'Université, Sherbrooke, Québec J1K 2R1, Canada

<sup>3</sup> Canadian Institute for Advanced Research, Toronto, Ontario M5G 1Z8, Canada

**Abstract.** Quantum state transfer into a memory, state shuttling over long distances via a quantum bus, and high-fidelity readout are important tasks for quantum technology. Realizing these tasks is challenging in the presence of realistic couplings to an environment. Here, we introduce and assess protocols that can be used in cavity QED to perform high-fidelity quantum state transfer and fast quantum nondemolition qubit readout through Hamiltonian engineering. We show that high-fidelity state transfer between a cavity and a single qubit can be performed, even in the limit of strong dephasing due to inhomogeneous broadening. We generalize this result to state transfer between a cavity and a logical qubit encoded in a collective mode of a large ensemble of  $N$  physical qubits. Under a decoupling sequence, we show that inhomogeneity in the ensemble couples two collective bright states to only two other collective modes, leaving the remaining  $N - 3$  single-excitation states dark. Moreover, we show that large signal-to-noise and high single-shot fidelity can be achieved in a cavity-based qubit readout, even in the weak-coupling limit. These ideas may be important for novel systems coupling single spins to a microwave cavity.

## 1. Introduction

Spin qubits encoded in collective modes of ensembles [1, 2, 3] and single spins in quantum dots [4, 5, 6] can be coupled to microwave cavities for cavity quantum electrodynamics (QED) experiments [7]. Spin qubits show promise for use as long-lived quantum memories, but often suffer from weak qubit-cavity coupling relative to the inhomogeneously broadened linewidth [8]. Inhomogeneous broadening typically originates from nuclear-spin or electrical (charge) noise [9, 10, 11, 12]. While nuclear-spin noise [13] can often be controlled through isotopic purification, strong coupling of a single spin to the electric field of a cavity mode typically requires a strong correlation of spin and charge degrees of freedom [14, 15, 16, 17, 18]. This correlation makes the spin qubit susceptible to low-frequency charge noise [19, 20]. An alternative strategy is to enhance the weak magnetic coupling of a spin qubit (which may be otherwise insensitive to charge noise) by coupling to the collective mode of a large spin ensemble [21, 22]. However, spatial inhomogeneities in such ensembles can result in an inhomogeneous linewidth that is comparable to the qubit-cavity coupling [3, 23].

It is well known that the effects of inhomogeneous broadening can be eliminated through a suitable dynamical decoupling sequence. To determine the quality of a cavity-QED scheme, the coupling is therefore often compared with the inverse qubit coherence time under a train of decoupling  $\pi$ -pulses [14, 15, 16], rather than the inhomogeneous linewidth. However, for a qubit coupled to a cavity, a sequence of  $\pi$ -pulses typically generates unwanted cavity excitations on the same timescale as coherent qubit-cavity oscillations, severely reducing the fidelity of, e.g., quantum state transfer between a qubit and a cavity.

In this paper, we show that these limitations can be overcome by engineering appropriate time-averaged Hamiltonians [24, 25, 26, 27] through a combination of qubit dynamical decoupling and control of the qubit-cavity coupling. In particular, we introduce and quantitatively characterize protocols for a high-fidelity quantum state transfer between a qubit and cavity, and for a fast quantum nondemolition qubit readout. Our readout protocol yields a large signal-to-noise ratio even in the weak-coupling regime, in which the qubit-cavity coupling is small compared to the cavity damping rate. Moreover, we show that control of the qubit-cavity coupling makes high-fidelity quantum state transfer possible even in the strong-dephasing limit, in which the inhomogeneous linewidth dominates the qubit-cavity coupling. This result applies even to logical qubits encoded in the collective mode of an ensemble of physical qubits (relevant to, e.g., spin or atomic ensembles that are routinely used for quantum memories [3, 28, 29]). Inhomogeneous broadening across an uncontrolled ensemble of  $N$  physical qubits would typically lead to coupling of the logical qubit to  $\sim N$  collective modes [23, 30, 31]. However, remarkably, for our pulse sequence we find that the leading corrections in average Hamiltonian theory couple only four distinct collective modes in the large- $N$  limit. This may allow for very high-fidelity storage-and-retrieval or even coherent manipulation of quantum information in the ensemble through revivals.

This paper is organized as follows. In Section 2, we introduce the Hamiltonian engineering protocol studied throughout this work. In Section 3, we evaluate the fidelity of a quantum state transfer between a cavity and a single physical qubit under the Hamiltonian-engineering protocol presented here, and show that errors can be strongly suppressed, even in the strong-dephasing limit (in which the inhomogeneous broadening is larger than the qubit-cavity coupling). In Section 4, we generalize this

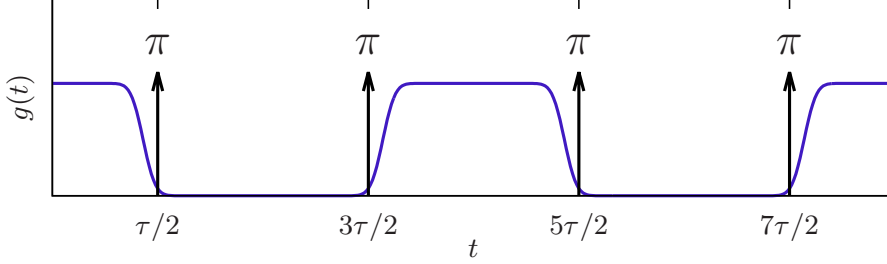


**Figure 1.** SQUADD (SQUare wave And Dynamical Decoupling): the Carr-Purcell sequence is applied to a qubit coupled to a cavity while turning off the coupling  $g(t)$  [Eq. (4)] after each odd-numbered  $\pi$ -pulse to prevent unwanted cavity excitations.

result to state transfer between a cavity and a collective mode of a large ensemble of physical qubits. In Section 5, we present a scheme to avoid accumulation of error arising under deterministic over (under)-rotations of the qubit during imperfect  $\pi$  pulses. Finally, in Section 6, we show how a simple modification of the dynamical decoupling sequence introduced here leads to a readout protocol yielding high signal-to-noise and single-shot fidelity in the weak-coupling regime.

## 2. Hamiltonian engineering

We first consider a single qubit coupled to a cavity. With the cavity and the qubit on resonance and working in a rotating frame within the rotating-wave approximation  $\ddagger$ , the system is described by a Jaynes-Cummings Hamiltonian:

$$H_{\text{JC}}(t) = \xi \sigma_z / 2 + g(t)(a^\dagger \sigma_- + a \sigma_+), \quad (1)$$

where we have allowed for a tunable qubit-cavity coupling  $g(t)$  (setting  $\hbar = 1$ ). In addition, the qubit is controlled via  $H_c(t)$ , giving the total Hamiltonian

$$H(t) = H_{\text{JC}}(t) + H_c(t). \quad (2)$$

In  $H_{\text{JC}}(t)$ , we take  $\xi$  to be a Gaussian random variable with zero mean and variance  $(\Delta\xi)^2$  that describes inhomogeneous broadening in the qubit-cavity detuning. Most decoupling schemes rely entirely on qubit control. However, electrical control of  $g(t)$  is now possible in several architectures [32, 33, 34, 16, 5]. By modulating  $H_c(t)$  and  $g(t)$  sufficiently quickly, we can eliminate unwanted terms and generate useful time-averaged Hamiltonians.

To average away unwanted terms, we move to the toggling frame [35], which incorporates  $H_c(t)$  into the transformed system Hamiltonian,

$$H_{\text{T}}(t) = U_c^\dagger(t) H_{\text{JC}}(t) U_c(t), \quad (3)$$

where  $U_c(t) = \mathcal{T} \exp[-i \int_0^t dt' H_c(t')]$ . To reduce dephasing due to the random detuning  $\xi$ , a natural choice for  $U_c(t)$  is the Carr-Purcell sequence: a train of sharp  $\pi$ -pulses applied at times  $(m + \frac{1}{2})\tau$ , with  $m \in \mathbb{N}$  (Fig. 1). In this case,

$\ddagger$  See Appendix B for a discussion of the effect of counter-rotating terms and finite-bandwidth control.

$$H_T(t) = \begin{cases} \frac{1}{2}\xi\sigma_z + g(t)[a^\dagger\sigma_- + a\sigma_+], & n(t) \text{ even}, \\ -\frac{1}{2}\xi\sigma_z + g(t)[a^\dagger\sigma_+ + a\sigma_-], & n(t) \text{ odd}, \end{cases} \quad (4)$$

with  $n(t)$  the number of  $\pi$ -pulses applied before time  $t$ . For  $n(t)$  even, the qubit-cavity interaction is described by a co-rotating term, preserving the total number of excitations,  $N_{\text{ex}} \equiv a^\dagger a + \sigma_+ \sigma_-$ . However, for  $n(t)$  odd, the interaction is rather given by a counter-rotating term, which does not conserve  $N_{\text{ex}}$ . For fixed  $g(t) = g$ , the counter-rotating term leads to simultaneous excitation of the qubit and cavity on a time scale comparable to the state-transfer time. This flow of excitations can be blocked simply by taking  $g(t) = 0$  for  $n(t)$  odd. With this choice,  $N_{\text{ex}}$  is a constant of motion, allowing for coherent state transfer between the qubit and the Hilbert space spanned by the vacuum and first excited state of the cavity. As we show below, taking  $g(t) = g \forall t$  would rather lead to a fast qubit readout via the cavity.

### 3. Qubit-cavity state transfer

In the rest of this paper, we will use the acronym SQUADD (SQUare wave And Dynamical Decoupling) to describe the simultaneous square-wave modulation of  $g(t)$  and sequence of  $\pi$ -pulses shown in Fig. 1. If this sequence were not applied, inhomogeneous broadening  $\Delta\xi$  of the order of  $g \equiv \max_t[g(t)]$  would result in a state-transfer error (infidelity) of order 1. However, under SQUADD with a sufficiently short period  $2\tau$ , the system dynamics are accurately described by the average Hamiltonian

$$\bar{H}^{(0)} = \frac{1}{2\tau} \int_0^{2\tau} dt H_T(t) = \bar{g}(a^\dagger\sigma_- + a\sigma_+), \quad (5)$$

where we have introduced the average coupling,  $\bar{g} \equiv \int_0^{2\tau} dt g(t)/2\tau$ . In Eq. (5),  $\bar{H}^{(0)}$  is the leading term in average Hamiltonian theory, which recasts the evolution operator  $U(t) = \mathcal{T} \exp[-i \int_0^t dt' H_T(t')]$  in terms of a Magnus expansion [36, 37]:

$$U(t) = \exp \left[ -it \sum_{k=0}^{\infty} \bar{H}^{(k)} \right]. \quad (6)$$

Complete state transfer is achieved at a final transfer time  $t_f$ , where

$$\bar{g}t_f = \bar{g}n_p\tau = \frac{\pi}{2}, \quad (7)$$

and  $n_p$  is the total number of  $\pi$ -pulses. Importantly, this condition for state transfer is independent of the precise shape of  $g(t)$ , as long as  $g(t) = 0$  for  $n(t)$  odd. The Magnus expansion converges rapidly when

$$\int_0^{2\tau} dt \|H_T(t)\|_2 \lesssim \max(\bar{g}, \Delta\xi)2\tau \ll 1. \quad (8)$$

Equivalently, for a fixed transfer time  $t_f = n_p\tau = \pi/2\bar{g}$ ,  $n_p \gg \pi \max(1, \Delta\xi/g)$ .

Equation (5) gives an exact description of the time evolution in the limit  $\tau \rightarrow 0$ . However, in practice,  $\tau$  will always be limited by the bandwidth of  $g(t)$  and the duration of  $\pi$  pulses. Thus, to characterize the performance of SQUADD, we evaluate the average fidelity

$$F = \int d\psi \langle \psi | U_0^\dagger \mathcal{M}(|\psi\rangle\langle\psi|) U_0 | \psi \rangle. \quad (9)$$

The integral in Eq. (9) represents an average with respect to the Haar measure  $d\psi$  (a uniform average over the Bloch sphere) for the ensemble of states of the form  $|\psi\rangle \equiv |\psi\rangle_q |0\rangle_c$ , where  $|\psi\rangle_q$  is an arbitrary pure qubit state and  $|0\rangle_c$  is the cavity vacuum. We have also introduced the unitary operator  $U_0$  describing an ideal state transfer:  $U_0|\psi\rangle_q |0\rangle_c = |g\rangle_q |\psi\rangle_c$ , with  $|g\rangle_q$  the qubit ground state. In addition,  $\mathcal{M}$  is the completely positive trace-preserving map that describes the actual state transfer for finite  $\tau$ , accounting for an average over the random detuning  $\xi$  and a finite cavity damping rate  $\kappa$ . We first consider the case  $\kappa = 0$ , then generalize to finite  $\kappa$ , below.

When  $g(t) = 0$  for  $n(t)$  odd,  $H_T(t)$  preserves the number of excitations  $N_{\text{ex}}$ . For fixed detuning  $\xi$ , the map  $\mathcal{M}$  can then be expressed in terms of a unitary, introducing a trivial phase on the state with  $N_{\text{ex}} = 0$  and a  $\xi$ -dependent  $\text{SU}(2)$  rotation in the two-dimensional space of  $N_{\text{ex}} = 1$  §. We take  $g(t) = g$  identically for  $n(t)$  even and expand to leading (fourth) order in  $\tau = \pi/gn_p$ . For  $\max(\Delta\xi, g)\tau \ll 1$  [equivalently,  $n_p \gg \pi \max(1, \Delta\xi/g)$ ], the error is then well-approximated by

$$1 - F \simeq \frac{1}{6} \left[ \left( \frac{\pi}{4} \right)^2 \left( \frac{\Delta\xi}{g} \right)^4 + \frac{1}{3} \left( \frac{\Delta\xi}{g} \right)^2 \right] \left( \frac{\pi}{2n_p} \right)^4. \quad (10)$$

The error ( $1 - F \propto 1/n_p^4$ ) is thus strongly suppressed with an increasing number of  $\pi$ -pulses, as shown in Fig. 2. Given a finite off/on ratio  $g_{\text{off}}/g$  [where  $g(t) = g_{\text{off}}$  for  $n(t)$  odd], we find a correction to the error of order  $\sim (g_{\text{off}}/g)^2$ . This term would ultimately limit the saturation fidelity at large  $n_p$  whenever  $g_{\text{off}} \neq 0$ .

Taking  $g_{\text{off}}/g = 0$ , a small error can be reached when  $n_p \gg 1$ , even for strong dephasing,  $gT_2^* = \sqrt{2}g/\Delta\xi < 1$ , where  $T_2^*$  is the qubit free-induction decay time (dephasing time) due to inhomogeneous broadening  $\Delta\xi$ . This result is apparent in Fig. 2, which gives the average error  $1 - F$  as a function of the total pulse number  $n_p = t_f/\tau = \pi/g\tau$  obtained from the exact solution described above (solid purple line), along with the large- $n_p$  expansion of Eq. (10) (dashed black line). Here, we have chosen  $gT_2^* = 1/10$ . Even for this choice of parameters, placing the system in the strong-dephasing regime, errors smaller than 1% are reached with  $n_p \sim 40$  pulses, at the onset of the validity criterion for Eq. (10):  $n_p > \pi\Delta\xi/g \sim 40$ . Consequently, the usual weak-dephasing criterion ( $1/T_2^* \ll g$ ) has been traded for a fast-control requirement ( $\tau \ll T_2^*$ ). Fast  $\pi$ -pulses in this limit have already been demonstrated with isolated spin qubits (not coupled to cavities) [13, 19, 38], and could in principle be made even faster for single spins by taking advantage of exchange coupling and the magnetic field gradient generated by a micromagnet [39, 40]. Since  $g(t)$  can be controlled electrically when these systems are coupled to cavities [5], fast pulsing of  $g(t)$  may be possible in the very near future (we give an analysis of finite-bandwidth control for  $g(t)$  and the influence of counter-rotating terms in Appendix B).

When  $n_p \rightarrow \infty$ , inhomogeneous broadening becomes irrelevant and the fidelity will ultimately be limited by cavity damping at rate  $\kappa$  (we neglect the homogeneous qubit decay under the decoupling sequence when  $\kappa T_2 > 1$ ). We find that the error saturates at

$$1 - F = \frac{\pi}{6} \frac{\kappa}{g} + \mathcal{O}\left(\frac{\kappa^2}{g^2}\right) \quad (11)$$

when  $n_p \rightarrow \infty$ . To illustrate this, we numerically solve the Lindblad master equation generated by a Liouvillian  $\mathcal{L}$  accounting for both Hamiltonian evolution under Eq. (4)

§ See Appendix A for the exact solution for state transfer using SQUADD.

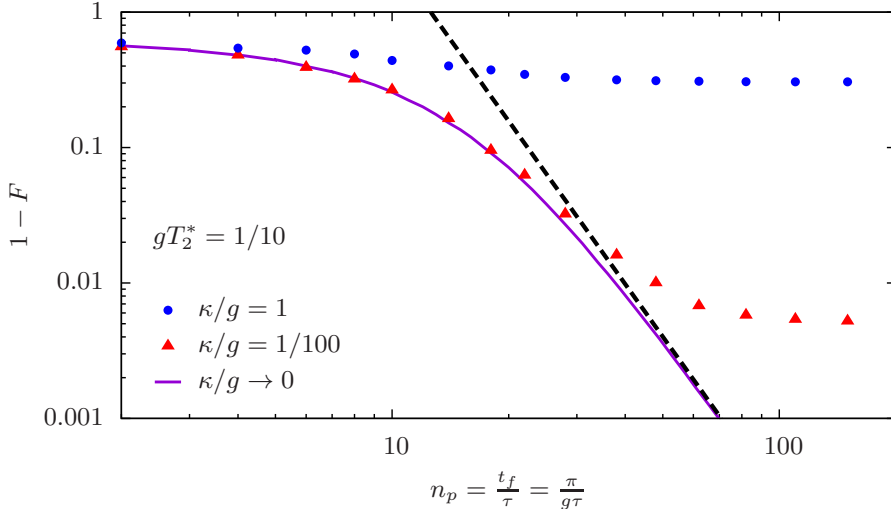


**Figure 2.** Suppression of state-transfer error  $1 - F$  with increasing number of pulses  $n_p$  for  $gT_2^* = \sqrt{2}g/\Delta\xi = 1/10$ . Dashed black line: Eq. (10). Solid purple line: exact solution, without cavity damping. Blue dots: exact numerical master-equation simulation including cavity damping, with  $\kappa/g = 1$ . Red triangles:  $\kappa/g = 1/100$ .

and cavity damping. As shown in Fig. 2, cavity damping does indeed lead to a saturation of the error as a function of  $n_p$  at  $1 - F \sim \kappa/g$  (blue dots:  $\kappa/g = 1$ , red triangles:  $\kappa/g = 1/100$ ).

As a concrete example, a coupling  $g/2\pi \simeq 1$  MHz has been predicted for spin qubits in GaAs double quantum dots [15], leading to  $gT_2^* \simeq 0.05$  due to hyperfine coupling to nuclear spins [13]. Even in this case, SQUADD could enable coherent coupling between a single spin and a cavity. In addition, SQUADD could improve state transfer between a single spin confined in a carbon nanotube and a coplanar-waveguide resonator. In a recent experiment on this system,  $g/2\pi = 1.3$  MHz,  $\kappa/2\pi = 0.6$  MHz, and  $T_2^* \simeq 60$  ns have been reported [5]. With these parameters, a large state-transfer error  $1 - F \simeq 0.42$  results from Eq. (9) without  $\pi$ -pulses. Using SQUADD,  $n_p = 10$  ( $\tau = \frac{\pi}{gn_p} \simeq 40$  ns) suffices to reduce the error from pure dephasing to 0.004. The total error is then  $1 - F \simeq 0.18$ , limited by the large  $\kappa/g$  ratio in this experiment.

#### 4. Collective modes in qubit ensembles

In this section, we consider the application of SQUADD to quantum state transfer between a cavity and a collective mode of an ensemble of  $N$  physical qubits. We account for leading corrections in the Magnus expansion and show that, up to corrections  $\sim \mathcal{O}(1/\sqrt{N})$ , this system evolves in a closed 4-dimensional subspace. Using this approach, we retrieve an expression similar to Eq. (10) for the state-transfer fidelity.

For single spins coupled to microwave cavities, the  $\kappa/g$  ratio can be large [41, 5], limiting the fidelity achievable through SQUADD. However, the effective coupling can be significantly enhanced by encoding a logical qubit into a large number of physical qubits. Indeed, an ensemble of  $N$  qubits coupled to a common cavity mode hosts an excitation out of the ground state  $|g\rangle_q = |g\rangle_1 \otimes |g\rangle_2 \cdots |g\rangle_N$  that is annihilated by the

collective lowering operator

$$b = \sum_{i=1}^N \frac{g_i}{\sqrt{N}g_{\text{av}}} \sigma_i^-, \quad g_{\text{av}} \equiv \sqrt{\sum_{i=1}^N \frac{g_i^2}{N}} \quad (12)$$

where  $g_i$  is the coupling for qubit  $i$ . For  $N \gg 1$ , the logical qubit encoded in the subspace of  $|g\rangle_q$  and  $|e\rangle_q = b^\dagger |g\rangle_q$  couples to the resonator with an ensemble coupling  $g_{\text{ens}} \equiv \sqrt{N}g_{\text{av}}$  [21]. However, an inhomogeneity in qubit-cavity detunings across the ensemble may lead to leakage from the collective mode  $b$  to many dark states [30, 31, 23]. When  $\Delta\xi \gtrsim g_{\text{ens}}$ , leakage due to dephasing will typically result in an error of order one.

Errors due to inhomogeneous broadening in an ensemble can be suppressed through SQUADD. The toggling-frame Hamiltonian for a qubit ensemble is

$$H_{\text{T}}(t) = \begin{cases} \frac{1}{2} \sum_i \xi_i \sigma_i^z + \sum_i g_i (a^\dagger \sigma_i^- + a \sigma_i^+), & n(t) \text{ even,} \\ -\frac{1}{2} \sum_i \xi_i \sigma_i^z, & n(t) \text{ odd.} \end{cases} \quad (13)$$

We thus consider an ensemble of qubits with couplings  $g_i(t)$  and detunings  $\xi_i$  from the cavity. As in the single-qubit case, we assume that  $g_i(t) = g_i \forall i$  for  $n(t)$  even and  $g_i(t) = 0 \forall i$  for  $n(t)$  odd. The time-dependent Hamiltonian in Eq. (13) describes rapid periodic modulation for small pulse interval  $\tau$ . For  $\max(g_{\text{ens}}, \Delta\xi)\tau \ll 1$  [equivalently,  $n_p \gg \max(\pi, \Delta\xi/g_{\text{ens}})$ ], the Magnus expansion converges rapidly, allowing us to truncate the expansion at leading and first subleading order. Because we have assumed  $g(t) = 0$  for  $n(t)$  odd, the total number of excitations  $N_{\text{ex}} = a^\dagger a + \sum_i \sigma_i^+ \sigma_i^-$  is a constant of motion. We thus project each  $\bar{H}^{(k)}$  into the subspace  $\mathcal{H}_{01}$  associated with  $N_{\text{ex}} = 0$  or 1. Explicitly,  $\mathcal{H}_{01}$  is spanned by the states  $|g\rangle_q \otimes |0\rangle_c$ ,  $|g\rangle_q |1\rangle_c$ , and  $|g\rangle_1 \otimes |g\rangle_2 \cdots |e\rangle_j \cdots |g\rangle_N \otimes |0\rangle_c$ , where 0 and 1 label cavity Fock states, and where  $|g\rangle_j$  and  $|e\rangle_j$  label the ground state and excited state of qubit  $j$ , respectively. We then have

$$\bar{H}^{(0)} = \frac{g_{\text{ens}}}{2} (a^\dagger b + ab^\dagger), \quad \bar{H}^{(1)} = 0, \quad (14)$$

$$\bar{H}^{(2)} = \Omega_1 (b^\dagger c + c^\dagger b) + \Omega_2 (a^\dagger d + d^\dagger a) + \chi a^\dagger a. \quad (15)$$

In Eqs. (14) and (15), we have introduced two new collective qubit lowering operators

$$c = \frac{1}{\sqrt{N}} \sum_i \frac{g_i \xi_i}{(g\xi)_{\text{av}}} \sigma_i^-, \quad (g\xi)_{\text{av}} = \sqrt{\sum_i \frac{g_i^2 \xi_i^2}{N}}, \quad (16)$$

$$d = \frac{1}{\sqrt{N}} \sum_i \frac{g_i \xi_i^2}{(g\xi^2)_{\text{av}}} \sigma_i^-, \quad (g\xi^2)_{\text{av}} = \sqrt{\sum_i \frac{g_i^2 \xi_i^4}{N}}. \quad (17)$$

Equation (15) describes the coupling of modes  $a$  and  $b$  with the new modes  $c$  and  $d$  with strengths

$$\Omega_1 = -\frac{N\tau^2}{48} g_{\text{av}} (g\xi)_{\text{av}}, \quad \Omega_2 = -\frac{\sqrt{N}\tau^2}{48} (g\xi^2)_{\text{av}}. \quad (18)$$

In addition, Eq. (15) contains a resonator shift by frequency

$$\chi = \frac{\tau^2}{24} \sum_i g_i^2 \xi_i. \quad (19)$$

By construction, after projecting into  $\mathcal{H}_{01}$ , the collective qubit operators obey the commutation relations

$$[b, b^\dagger] = [c, c^\dagger] = [d, d^\dagger] = 1 + \mathcal{O}(1/N). \quad (20)$$

Therefore, in the large- $N$  limit, the Hamiltonian  $\bar{H}^{(0)} + \bar{H}^{(2)}$  can be expanded in the basis of single-excitation states  $|m\rangle \equiv m^\dagger(|g\rangle_q \otimes |0\rangle_c)$ , where  $m \in \{a, b, c, d\}$ . However, this basis is typically non-orthogonal. To see this, we assume that the coupling strengths  $g_i$  are uncorrelated with the detunings  $\xi_i$ , implying that, e.g.,  $(g\xi)_{\text{av}} \rightarrow g_{\text{av}}\xi_{\text{av}}$  for  $N \rightarrow \infty$ . We also assume that the distribution of qubit-resonator detunings is Gaussian with mean  $E[\xi_i] = 0$ . Projecting into  $\mathcal{H}_{01}$ , this gives

$$[b, c^\dagger] = \mathcal{O}(1/\sqrt{N}), \quad [c, d^\dagger] = \mathcal{O}(1/\sqrt{N}), \quad (21)$$

$$[b, d^\dagger] = 1/\sqrt{3} + \mathcal{O}(1/\sqrt{N}), \quad (22)$$

all other relevant commutators between different modes being 0. Though  $[b, c^\dagger]$  and  $[c, d^\dagger]$  are suppressed in the large- $N$  limit,  $[b, d^\dagger]$  always remains of order 1. This implies that

$$s \equiv \langle b|d\rangle = \langle 0|[b, d^\dagger]|0\rangle = 1/\sqrt{3} + \mathcal{O}(1/\sqrt{N}). \quad (23)$$

To avoid the complications associated with the non-orthogonal basis  $\{|a\rangle, |b\rangle, |c\rangle, |d\rangle\}$ , we introduce a new set of single-excitation states  $\{|\tilde{a}\rangle, |\tilde{b}\rangle, |\tilde{c}\rangle, |\tilde{d}\rangle\}$ , where

$$|\tilde{a}\rangle = |a\rangle, \quad |\tilde{c}\rangle = |c\rangle, \quad (24)$$

$$|\tilde{b}\rangle = -\frac{1}{\sqrt{2(1-s)}}|b\rangle + \frac{1}{\sqrt{2(1-s)}}|d\rangle, \quad |\tilde{d}\rangle = \frac{1}{\sqrt{2(1+s)}}|b\rangle + \frac{1}{\sqrt{2(1+s)}}|d\rangle. \quad (25)$$

The states given in Eq. (24) and (25) form an orthonormal basis if we neglect overlaps  $\sim \mathcal{O}(1/\sqrt{N})$ . Writing a matrix representation of  $\bar{H}^{(0)} + \bar{H}^{(2)}$  in this basis, we find

$$[\bar{H}^{(0)} + \bar{H}^{(2)}] = \begin{pmatrix} 0 & \omega_- & 0 & \omega_+ \\ \omega_- & 0 & \omega'_+ & 0 \\ 0 & \omega'_+ & 0 & \omega'_- \\ \omega_+ & 0 & \omega'_- & 0 \end{pmatrix} [1 + \mathcal{O}(1/\sqrt{N})]. \quad (26)$$

In Eq. (26), we have introduced couplings between the orthonormal modes  $\tilde{a}$ ,  $\tilde{b}$ ,  $\tilde{c}$ , and  $\tilde{d}$ , given by

$$\omega_\pm = \pm \sqrt{\frac{1 \pm s}{2}} \left[ \frac{g_{\text{ens}}}{2} \mp \frac{1}{48} g_{\text{ens}} (\xi^2)_{\text{av}} \tau^2 \right], \quad \omega'_\pm = \pm \frac{1}{48} \sqrt{\frac{1 \mp s}{2}} g_{\text{ens}}^2 \xi_{\text{av}} \tau^2. \quad (27)$$

Assuming  $N \gg 1$ , we neglect corrections  $\sim \mathcal{O}(1/\sqrt{N})$ . The Hamiltonian in Eq. (26) can then be represented graphically, as shown in Fig. 3(b). For  $\Delta\xi\tau = 0$ , Eq. (27) yields  $\omega'_\pm = 0$ . The Hamiltonian then has the structure of a  $\Lambda$  system, with a basis state  $|\tilde{a}\rangle$  coupled to the two basis states  $|\tilde{b}\rangle$  and  $|\tilde{d}\rangle$ . These couplings are represented by the thick red arrows in Fig. 3(b). In this limit, the Hamiltonian in Eq. (26) has two bright eigenstates with energy  $\pm g_{\text{ens}}/2$ . This is clearly seen in Fig. 3(a), which shows the eigenenergies of the Hamiltonian in Eq. (26) as a function of  $\Delta\xi\tau$ , where  $\Delta\xi$



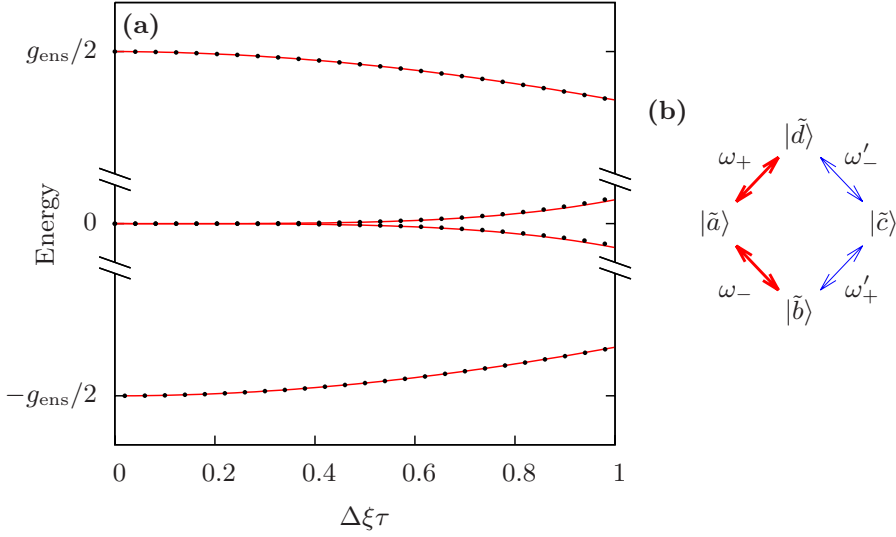


**Figure 3.** Spectrum of the time-independent effective Hamiltonian  $\bar{H}^{(0)} + \bar{H}^{(2)}$  for a qubit ensemble coupled to a resonator under SQUADD. (a) Eigenenergies as a function of  $\Delta\xi\tau$ , where  $\Delta\xi$  is the standard deviation of the Gaussian distribution of qubit-resonator detunings  $\xi_i$ , and  $\tau$  is the dynamical-decoupling pulse interval. Solid red line: eigenenergies obtained by analytically diagonalizing the effective  $4 \times 4$  Hamiltonian in Eq. (26), dropping corrections  $\sim \mathcal{O}(1/\sqrt{N})$  (see Appendix C). Black dots: exact numerical diagonalization of  $\bar{H}^{(0)} + \bar{H}^{(2)}$  given by Eqs. (14) and Eq. (15), which include corrections  $\sim \mathcal{O}(1/\sqrt{N})$ . We take  $g_{\text{ens}} = \Delta\xi$ , and  $N = 1000$ . (b) Couplings between the basis states  $\{|\tilde{a}\rangle, |\tilde{b}\rangle, |\tilde{c}\rangle, |\tilde{d}\rangle\}$ , as given by Eq. (26).

is the standard deviation of the Gaussian distribution of qubit-resonator detunings. For  $\Delta\xi\tau = 0$ , all other  $N - 1$  eigenstates are zero-energy dark states which do not couple to the resonator mode. In contrast, when  $\Delta\xi\tau > 0$ , the Hamiltonian has the structure of a tight-binding problem on a ring; the basis states  $|\tilde{b}\rangle$  and  $|\tilde{d}\rangle$  become weakly coupled through an additional mode  $|\tilde{c}\rangle$ . These additional hopping terms are represented by the thin blue arrows in Fig. 3(b). Because of the simple tridiagonal form of the Hamiltonian in Eq. (26), we are able to find analytic expressions for the eigenenergies and eigenstates of  $\bar{H}^{(0)} + \bar{H}^{(2)}$  for  $\Delta\xi\tau > 0$ . These expressions are given in Appendix C. As shown in Fig. 3(a) by the solid red lines, introducing couplings to the mode  $|\tilde{c}\rangle$  by turning on  $\Delta\xi$  shifts the energies of the two initial bright states, and lifts the degeneracy between two of the initial dark states by coupling them to the resonator mode. These two effects will generate errors in the state transfer of the resonator quantum state into the ensemble of qubits.

We characterize errors in SQUADD due to inhomogeneous broadening with the average fidelity  $F$ , as defined in Eq. (9). We consider the initial state  $|\psi\rangle \equiv |g\rangle_{\text{q}} \otimes |\psi\rangle_{\text{c}}$ , where  $|\psi\rangle_{\text{c}}$  is an arbitrary superposition of the cavity states  $|0\rangle_{\text{c}}$  and  $|1\rangle_{\text{c}}$ . We choose the evolution operator for an ideal state transfer to be  $U_0 = -ib^\dagger a$ , where the  $-i$  phase factor appears because the state transfer described here is equivalent to an  $\text{SU}(2)$  rotation. We take the linear map  $\mathcal{M}$  representing imperfect state transfer to correspond to the evolution operator under the effective time-independent Hamiltonian in Eq. (26). We perform a Taylor expansion of the resulting fidelity to leading (fourth)

order in  $\tau$ , assuming  $\max(g_{\text{ens}}, \Delta\xi)\tau \ll 1$ . Using the condition for complete state transfer,  $\tau = \pi/g_{\text{ens}}n_p$ , this assumption becomes  $n_p \gg \max(\pi, \Delta\xi/g_{\text{ens}})$ , resulting in

$$1 - F \simeq \left[ \frac{8 + \pi^2}{18} \left( \frac{\Delta\xi}{2g_{\text{ens}}} \right)^4 + \frac{1}{18} \left( \frac{\Delta\xi}{2g_{\text{ens}}} \right)^2 \right] \left( \frac{\pi}{2n_p} \right)^4. \quad (28)$$

We recall that we have dropped corrections of  $\mathcal{O}(1/\sqrt{N})$  arising from overlaps between basis states. Ignoring numerical prefactors of order 1, Eq. (28) exactly corresponds to Eq. (10) for a single qubit, after the replacement  $g \rightarrow g_{\text{ens}}$ . In Eq. (28), the numerical prefactors (obtained for  $N \gg 1$ ) differ from those obtained in Eq. (10) for  $N = 1$  because the mode structure is not the same. Indeed, taking  $N = 1$  in Eqs. (12), (16), and (17) leads to  $b = c = d = \sigma_-$ . The overlap between excitations of any pair of modes  $\in \{b, c, d\}$  is then  $\langle 0|\sigma_- \sigma_+|0\rangle = 1$ , in contradiction with the overlaps obtained from Eqs. (21) to (23) when neglecting terms  $\sim \mathcal{O}(1/\sqrt{N})$  for  $N \gg 1$ .

The above discussion shows that SQUADD is robust to inhomogeneous broadening, even when coupling a cavity to a collective mode. By modulating the detuning rather than the coupling, it may be possible to use a variation of SQUADD on ensembles of nitrogen vacancy (NV)-center spin qubits in diamond coupled to superconducting coplanar waveguides, for which  $\Delta\xi \sim g_{\text{ens}}$  has been reported [23].

This treatment of collective modes in qubit ensembles also demonstrates a clear advantage of our analytical approach over brute-force numerical methods for optimal control. Indeed, the time required for numerical exponentiation of the full system Hamiltonian grows exponentially with ensemble size, making the problem numerically challenging for  $N \gg 1$ . In contrast, the analytical approach reveals a closed 4-dimensional subspace in the same large- $N$  limit.

## 5. Pulse errors

In general, over-rotation or under-rotation of the qubit due to imperfect control can lead to an accumulation of errors as the number of pulses  $n_p$  is increased. A simple way to avoid accumulation of these pulse errors is to use a phase-alternated sequence [35], in which the qubit rotation direction alternates from one  $\pi$ -pulse to the next. Consequently, the (fixed, deterministic) error  $\varepsilon$  on the rotation angle of successive pulses cancels for  $n(t)$  even, but introduces a small over-rotation for  $n(t)$  odd. We evaluate the resulting correction  $\delta F$  to the state-transfer fidelity of Eq. (10) by expanding  $U(t) = \mathcal{T} \exp[-i \int_0^t dt' H_{\text{T}}(t')]$  to leading order in  $\varepsilon$  and in  $\tau$ . When  $\max(g, \Delta\xi)\tau \ll 1$ ,  $\delta F$  is then well-approximated by this leading correction:

$$\delta F \simeq -\frac{1}{2} \left( \frac{4}{3} - \frac{1}{\sqrt{2}} \sin \frac{\pi}{\sqrt{2}} \right) \left( \varepsilon \frac{\Delta\xi}{g} \right)^2. \quad (29)$$

Thus, neglecting order-unity prefactors, pulse errors can be made negligible compared to the error given in Eq. (10) when  $\varepsilon \ll \max \left[ (\Delta\xi/g)^2, 1 \right] / n_p^2$ .

## 6. Qubit readout

Recently, a longitudinal qubit-cavity interaction  $[\propto g(a^\dagger + a)\sigma_z]$  has been considered theoretically and shown to produce a quantum nondemolition readout that is faster

than the usual dispersive readout [42]. Here, we show how this type of interaction can be engineered through a simple modification of SQUADD. We investigate limits to the readout signal-to-noise and single-shot fidelity using this Hamiltonian-engineering approach, and find that these two measures can be large even in the weak-coupling regime ( $g < \kappa$ ).

If the Carr-Purcell sequence shown in Fig. 1 is applied with a fixed coupling,  $g(t) = g \forall t$ , the counter-rotating term in Eq. (4) contributes. Although this is harmful to state transfer, this term can also generate otherwise useful quantum operations. Indeed, the evolution operator from leading-order average Hamiltonian theory is then

$$U_R(t_f) = e^{-ig(a^\dagger + a)\sigma_x t_f/2} = D(-i\sigma_x g t_f/2), \quad (30)$$

where  $D(\alpha)$  is the displacement operator producing the coherent state  $|\alpha\rangle_c \equiv D(\alpha)|0\rangle_c$  [43]. The interaction appearing in Eq. (30) is longitudinal with respect to  $\sigma_x$  eigenstates,  $|\pm\rangle_q$ . Applying  $U_R(t_f)$  on  $|\pm\rangle_q$  then gives

$$U_R(t_f)|\pm\rangle_q|0\rangle_c = |\pm\rangle_q|\pm\alpha\rangle_c, \quad (31)$$

with  $\alpha \equiv -igt_f/2$ . Thus, in combination with a qubit rotation conditioned on the cavity state [44],  $U_R(t_f)$  can be used to map a qubit state to a superposition of cavity coherent states; a Schrödinger's cat state [45, 46]. Alternatively, the states  $|\pm\alpha\rangle_c$  can be resolved by homodyne detection of the signal leaking from the cavity, enabling quantum nondemolition readout of the qubit in the basis  $\{|\pm\rangle_q\}$ .

When a qubit is successively prepared and measured  $m \gg 1$  times to estimate an expectation value, the measurement statistics describing the mean of many independent repeated measurements become Gaussian. The performance of the readout proposed here is then well characterized by the signal-to-noise ratio (SNR). Indeed, the SNR compares the first two moments of the measurement operator

$$M = i\sqrt{\kappa} \int_0^{t_f} dt [a_{\text{out}}^\dagger(t) - a_{\text{out}}(t)], \quad (32)$$

the integrated homodyne-detection signal for a measurement time  $t_f$ , with  $a_{\text{out}}(t)$  the output field leaking from the cavity. We then take

$$\text{SNR} \equiv \frac{|\langle M \rangle_+ - \langle M \rangle_-|}{[\Delta M_+^2 + \Delta M_-^2]^{1/2}}, \quad (33)$$

where  $\Delta M_\pm^2 \equiv \langle M^2 \rangle_\pm - \langle M \rangle_\pm^2$  and where  $\langle O \rangle_\pm = \text{tr}[O(t_f)\rho_\pm]$ , with  $\rho_\pm = |\pm\rangle_q\langle\pm|_q \otimes |0\rangle_c\langle 0|_c$  [42]. To evaluate the maximum achievable SNR, it is important to account for the first two nonvanishing orders in the Magnus expansion for the time-periodic Liouvillian:  $\bar{\mathcal{L}} \simeq \bar{\mathcal{L}}^{(0)} + \bar{\mathcal{L}}^{(2)}$ . While  $\bar{\mathcal{L}}^{(0)}$  generates the required conditional coherent-state displacement,  $\bar{\mathcal{L}}^{(2)}$  results in qubit switching at a rate  $\Gamma \simeq g^2\tau^2\kappa/24$  in the basis  $\{|\pm\rangle_q\}$ . This qubit switching acts as a source of telegraph noise in the Langevin equation for the cavity field  $a(t)$  [47]. For  $g \ll \kappa$  and  $\kappa\tau \ll 1$ , this telegraph noise leads to a maximal value for the SNR §:

$$\text{SNR} \simeq \left(\frac{6g^2}{\kappa\Gamma}\right)^{1/4} \simeq \frac{2\sqrt{3}}{\sqrt{\kappa\tau}}. \quad (34)$$

Thus, for a short pulse interval,  $\kappa\tau < 1$ , this approach enables large SNR even in the weak-coupling regime ( $g < \kappa$ ), reducing additional noise (beyond projection noise) in the evaluation of qubit expectation values from a soft average [48, 49].

In contrast to the case of many repeated measurements (described above), for a single-shot readout, the measurement statistics are non-Gaussian. Indeed, while the conditional probability distribution describing the integrated signal  $\langle M \rangle_{\pm}$  would simply describe a displaced Gaussian in the absence of switching, random switching events (e.g. qubit decay due to the mechanism described above) lead to significant bimodality [50]. A good measure of quality is then the single-shot fidelity. In the same regime as above ( $g \ll \kappa$  and  $\kappa\tau \ll 1$ ), we apply the methods of Refs. [51, 50] and find a large single-shot fidelity

$$F_1 \simeq 1 - \frac{(\kappa\tau)^2}{192} \log \left[ \frac{96}{(\kappa\tau)^2} \right], \quad (35)$$

limited by the qubit switching mechanism described above §. For  $\kappa\tau = 0.1$ , this yields a single-shot fidelity of 99.95%. This type of readout may be useful in several novel experimental settings where it is challenging to achieve strong coupling. For example, a spin qubit in a carbon nanotube has recently been successfully coupled to a microwave resonator, but the coupling achieved is marginal,  $g/\kappa \sim 1$  [5]. Alternative setups for semiconductor spin qubits in quantum dots or at single donor impurities coupled to microwave cavities have predicted couplings  $g/2\pi \lesssim 1$  MHz [15, 41, 18], typically smaller than the damping rate  $\kappa/2\pi = 2$ -10 MHz [52, 53].

## 7. Conclusion

Moving forward, the ideas presented here could lead to applications well beyond state transfer and readout. For example, going to second order in average Hamiltonian theory yields terms  $\propto g^2\tau[a^2 + (a^\dagger)^2]$ , which could be used to generate cavity squeezing. Such squeezing may be useful, e.g., to further improve qubit readout [42]. In addition, by monitoring the coherence of a state that is periodically swapped between a qubit and a bosonic mode, it may be possible to characterize noise processes affecting a harmonic system (e.g., a cavity or a magnon mode [54]). This may generalize noise spectroscopy methods [55] to linear systems for which direct application of  $\pi$ -pulses is impossible.

## Acknowledgments

We thank Nicolas Didier, Benjamin d’Anjou, Michel Pioro-Ladrière, and Dany Lachance-Quirion for useful discussions. This research was undertaken thanks in part to funding from the Canada First Research Excellence Fund. This work was supported by NSERC, CIFAR, and the W. C. Sumner Foundation.

## Appendix A. Evolution under SQUADD

In this section, we derive the exact evolution operator that corresponds to the SQUADD state-transfer sequence, described in the main text. We assume that the

§ See Appendix D for a derivation of signal-to-noise and single-shot fidelity for the readout scheme proposed here.

qubit-resonator coupling strength  $g(t)$  is  $g$  for even  $n(t)$  and 0 for odd  $n(t)$ , where  $n(t)$  is the number of qubit  $\pi$  pulses applied before time  $t$ . The time-evolution operator then breaks into segments associated with the intervals of duration  $\tau$  between  $\pi$  pulses. In the subspace for which the total number of excitations  $N_{\text{ex}} = a^\dagger a + \sigma_+ \sigma_-$  has eigenvalue 1, the evolution operator for a single period of the decoupling sequence takes the form

$$U_1 = R_{\mathbf{n}}(\Omega\tau)R_{\mathbf{z}}(-\xi\tau)R_{\mathbf{n}}(\Omega\tau), \quad (\text{A.1})$$

with

$$\Omega = \sqrt{g^2 + \xi^2/4}, \quad (\text{A.2})$$

$$\mathbf{n} = \frac{g}{\Omega}\mathbf{x} + \frac{\xi}{2\Omega}\mathbf{z}. \quad (\text{A.3})$$

In the above equations,  $\xi$  is the random qubit-resonator detuning introduced above Eq. (4). In addition, in Eq. (A.1), we have introduced the operator  $R_{\mathbf{n}}(\theta) \equiv e^{-i\theta\mathbf{n}\cdot\boldsymbol{\tau}/2}$ , which applies an SU(2) rotation by angle  $\theta$  around the axis set by the unit vector  $\mathbf{n}$  in the space spanned by the vector of pseudospins  $\boldsymbol{\tau} = (\tau_x, \tau_y, \tau_z)$ . These pseudospins are defined by

$$\tau_x = |g1\rangle\langle e0| + |e0\rangle\langle g1|, \quad (\text{A.4})$$

$$\tau_y = i(|g1\rangle\langle e0| - |e0\rangle\langle g1|), \quad (\text{A.5})$$

$$\tau_z = |e0\rangle\langle e0| - |g1\rangle\langle g1|. \quad (\text{A.6})$$

In Eqs. (A.4) to (A.6),  $g$  ( $e$ ) labels the ground (excited) state of the qubit, while 0 or 1 is the number of photons in the cavity. The product of the three rotation matrices in Eq. (A.1) is itself a rotation matrix  $U_1 = R_{\mathbf{v}}(\vartheta)$ , where

$$\cos \frac{\vartheta}{2} = \sqrt{1 - A^2 - B^2}, \quad (\text{A.7})$$

$$\mathbf{v} = \frac{A}{\sqrt{A^2 + B^2}}\mathbf{x} + \frac{B}{\sqrt{A^2 + B^2}}\mathbf{z}, \quad (\text{A.8})$$

with

$$A = \frac{2g}{\Omega} \left( \cos \frac{\Omega\tau}{2} \cos \frac{\xi\tau}{2} + \frac{\xi}{2\Omega} \sin \frac{\Omega\tau}{2} \sin \frac{\xi\tau}{2} \right) \sin \frac{\Omega\tau}{2}, \quad (\text{A.9})$$

$$B = \left( \frac{\xi}{\Omega} \sin \frac{\Omega\tau}{2} \cos \frac{\xi\tau}{2} - \cos \frac{\Omega\tau}{2} \sin \frac{\xi\tau}{2} \right) \cos \frac{\Omega\tau}{2} + \frac{\xi^2 - 4g^2}{4\Omega^2} \sin^2 \frac{\Omega\tau}{2} \sin \frac{\xi\tau}{2}. \quad (\text{A.10})$$

The evolution at the end of the full sequence containing  $n_p$  pulses (and thus  $n_p/2$  periods) is given by

$$U(t_f) = U_1^{n_p/2} = R_{\mathbf{v}}(n_p\vartheta/2), \quad (\text{A.11})$$

for even  $n_p$ . Eq. (A.11) gives us a closed-form analytical expression for the evolution operator under the SQUADD sequence. Taking  $\mathcal{M}(|\psi\rangle\langle\psi|) = U(t_f)|\psi\rangle\langle\psi|U^\dagger(t_f)$  in Eq. (3) of the main text, with  $U(t_f)$  given by Eq. (A.11), we obtain the average state-transfer fidelity

$$F = \frac{1}{3} \text{E} \left[ 1 + v_x^2 \sin^2 \frac{n_p\vartheta}{4} + v_x \sin \frac{n_p\vartheta}{4} \right], \quad (\text{A.12})$$

where  $E[\cdot]$  is an ensemble average over the detuning  $\xi$ .

A simple analytical expression can be obtained for  $F$  when  $g\tau \ll 1$  and  $\xi\tau \ll 1$ . In this situation, we substitute Eqs. (A.9) and (A.10) into Eqs. (A.7) and (A.8), and expand the resulting expressions for  $\mathbf{v}$  and  $\vartheta/2$  to fourth order in  $\tau$ . In addition, we use the condition for complete state transfer  $\bar{g}t_f = (g/2)n_p\tau = \pi/2$ , where  $\bar{g}$  is the time average of the coupling strength on a period of the sequence and  $t_f$  is the transfer time. Assuming a Gaussian distribution of the detuning  $\xi$  with standard deviation  $\Delta\xi$ , we obtain Eq. (10), valid for  $g\tau \ll 1$  and  $\Delta\xi\tau \ll 1$ .

## Appendix B. Finite bandwidth and counter-rotating terms

We evaluate the state-transfer fidelity using numerical simulations that take into account both the finite bandwidth of the coupling modulation  $g(t)$  and the counter-rotating terms in the Rabi Hamiltonian. In these simulations, we find the evolution of the system under the toggling-frame Hamiltonian

$$H_T(t) = \begin{cases} H_T^{\text{even}}(t), & n(t) \text{ even}, \\ H_T^{\text{odd}}(t), & n(t) \text{ odd}. \end{cases} \quad (\text{B.1})$$

where

$$\begin{aligned} H_T^{\text{even}}(t) &= \frac{1}{2}\xi\sigma_z + g(t)[a^\dagger\sigma_- + a^\dagger\sigma_+e^{2i\omega_q t} + \text{H.c.}], \\ H_T^{\text{odd}}(t) &= -\frac{1}{2}\xi\sigma_z + g(t)[a^\dagger\sigma_+ + a^\dagger\sigma_-e^{2i\omega_q t} + \text{H.c.}], \end{aligned} \quad (\text{B.2})$$

with  $\omega_q$  the qubit frequency (the qubit and the resonator are resonant). In contrast with Eq. (4), Eqs. (B.2) take into account the counter-rotating terms appearing in the Rabi Hamiltonian. These terms give rise to leakage outside the subspace containing zero or one excitation when  $g(\omega) \equiv \int_{-\infty}^{\infty} dt \exp[i\omega t]g(t)$  has significant weight at  $\omega = 2\omega_q$ .

To take into account the finite bandwidth of the coupling modulations, we use

$$g(t) = \mathcal{F}^{-1}[g_{\text{id}}(\omega)f(\omega)], \quad (\text{B.3})$$

where

$$g_{\text{id}}(\omega) = \mathcal{F}[g_{\text{id}}(t)], \quad f(\omega) = \exp[-\omega^2/2\sigma_f^2]. \quad (\text{B.4})$$

In Eqs. (B.3) and (B.4),  $\mathcal{F}^{(-1)}$  is the (inverse) Fourier transform,  $g_{\text{id}}(t)$  is the ideal square wave described in the main text, and  $f(\omega)$  is a Gaussian filter with standard deviation  $\sigma_f$  which eliminates high-frequency components of  $g_{\text{id}}(t)$ . Evaluation of the transforms in Eq. (B.3) leads to

$$g(t) = \sum_{j=0}^{n_p/2} g_{\text{sq}}(t - 2j\tau), \quad (\text{B.5})$$

where  $g_{\text{sq}}(t)$  describes a single filtered square pulse centered around  $t = 0$ ,

$$g_{\text{sq}}(t) = \frac{g}{2} \left\{ \text{erf} \left[ \frac{\sigma_f}{\sqrt{2}} \left( t + \frac{\tau'}{2} \right) \right] - \text{erf} \left[ \frac{\sigma_f}{\sqrt{2}} \left( t - \frac{\tau'}{2} \right) \right] \right\}. \quad (\text{B.6})$$

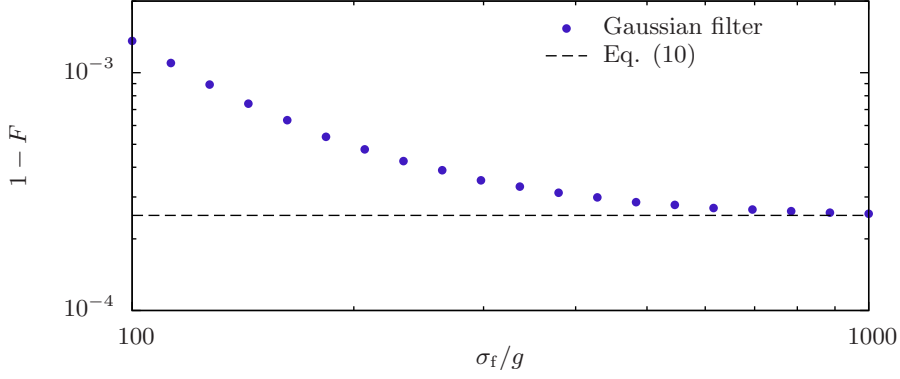


**Figure B1.** Error  $1-F$  due to finite pulse rise time in the square-wave modulation of  $g(t)$ . Blue dots: finite-bandwidth modulation obtained using a Gaussian filter with standard deviation  $\sigma_f$ . Dashed black line: error for perfectly square modulation of  $g(t)$ , given by Eq. (10). Parameters are:  $n_p = 100$ ,  $gT_2^* = 1/10$ ,  $\omega_q = 2000g$  and  $\kappa = 0$ .

In Eq. (B.6),  $\tau'$  is the width of the square coupling pulse, which may differ from the pulse interval  $\tau$ . The time required for the coupling to rise from 10 % to 90 % of its final value is, using Eq. (B.6),

$$t_r = \left[ \text{erf}^{-1} \left( \frac{9}{10} \right) - \text{erf}^{-1} \left( \frac{1}{10} \right) \right] \frac{\sqrt{2}}{\sigma_f} \simeq \frac{1.51919}{\sigma_f}. \quad (\text{B.7})$$

Taking  $\sigma_f < \omega_q$  allows to filter out the effect of the counter-rotating terms. Crucially, there is always the possibility for a separation between  $\omega_q$ ,  $\sigma_f$ , and  $1/\tau$ :

$$\omega_q > \sigma_f > \frac{1}{\tau}. \quad (\text{B.8})$$

When Eq. (B.8) is respected, the square wave is well approximated while still suppressing the effect of the counter-rotating terms.

To verify this, we numerically evaluate the fidelity of a state transfer using Eq. (3) of the main text, considering evolution under the toggling-frame Hamiltonian of Eq. (B.1). When the pulse rise time  $t_r$  is finite,  $g(t)$  becomes non-zero even for  $n(t)$  odd. To suppress the resulting unwanted excitations of the qubit and cavity, we then take  $\tau' = \tau - 2t_r$ , as illustrated in Fig. 1. Consequently, the time-averaged coupling  $\bar{g}$  also decreases; the pulse interval that results in a complete state transfer is then obtained by numerically solving  $\bar{g}n_p\tau = \pi/2$  for a given value of  $g$  and  $n_p$ . Taking  $n_p = 100$ ,  $gT_2^* = 1/10$ , and  $\kappa = 0$ , the resulting state-transfer error is shown in Fig. B1 as a function of  $\sigma_f/g$  (blue dots). As  $\sigma_f/g$  increases, the error decreases, approaching the value given by Eq. (10) for perfectly square modulation of  $g(t)$  (dashed black line). Additional error due to finite pulse rise time becomes negligible (for this choice of parameters) for  $\sigma_f \gtrsim 500g$ . Even for small bandwidth,  $\sigma_f < 500g$ , Fig. B1 shows that large overall suppression of error due to inhomogeneous broadening is possible (without SQUADD, error would be of order 1 for  $gT_2^* = 1/10$ ). In the simulations, we have taken  $\omega_q = 2000g$ . This choice allows us to filter out the effect of the counter-rotating terms in the whole parameter range of the simulation, for which

$\sigma_f < \omega_q$  is always satisfied. To give a concrete example, taking  $g/2\pi = 1$  MHz and  $\sigma_f = 100g$ , the parameters used in the simulation presented in Fig. B1 correspond to  $\sigma_f/2\pi = 100$  MHz,  $\omega_q/2\pi = 2$  GHz, and  $T_2^* \simeq 16$  ns. Numerically solving  $\bar{g}n_p\tau = \pi/2$  then gives  $\bar{g}/2\pi \simeq 0.42$  MHz and  $\tau \simeq 6$  ns for  $n_p = 100$ . Even for this narrow bandwidth (which leads to  $t_r \simeq 2.4$  ns), our simulation yields a relatively small error,  $1 - F \simeq 10^{-3}$ .

### Appendix C. Spectrum of the 4-dimensional Hamiltonian for state transfer to a collective mode in a qubit ensemble

In this Appendix, we give analytical expressions for the energy spectrum of the Hamiltonian of Eq. (26), which describes quantum state transfer between a cavity and a collective mode of an inhomogeneously broadened ensemble of physical qubits. Neglecting corrections  $\sim \mathcal{O}(1/\sqrt{N})$ , diagonalization of this Hamiltonian reveals two energy doublets: (i) a doublet of bright states (which have finite overlap with the cavity state  $|\bar{a}\rangle = |a\rangle = a^\dagger|0\rangle$ ), and (ii) a doublet of states which are dark (no overlap with  $|\bar{a}\rangle$ ) for  $\Delta\xi\tau = 0$ , but become bright for  $\Delta\xi\tau > 0$ . The eigenenergies corresponding to these two doublets are

$$E_{\pm}^{(i)} = \pm\sqrt{\frac{\omega_{\text{tot}}^2 + \Sigma^2}{2}}, \quad E_{\pm}^{(ii)} = \pm\sqrt{\frac{\omega_{\text{tot}}^2 - \Sigma^2}{2}}, \quad (\text{C.1})$$

respectively, where

$$\omega_{\text{tot}}^2 = \omega_+^2 + \omega_-^2 + (\omega'_+)^2 + (\omega'_-)^2, \quad (\text{C.2})$$

$$\Sigma^2 = \sqrt{[(\omega_+ + \omega'_+)^2 + (\omega_- - \omega'_-)^2][(\omega_+ - \omega'_+)^2 + (\omega_- + \omega'_-)^2]}. \quad (\text{C.3})$$

Expressions for  $\omega_{\pm}$  and  $\omega'_{\pm}$  are given in Eq. (27).

### Appendix D. Readout signal-to-noise ratio

We evaluate the optimal signal-to-noise ratio for the readout scheme introduced in the main text using standard input-output theory [47]. To define the signal-to-noise ratio, it is useful to introduce the operator [42]

$$M = i\sqrt{\kappa} \int_0^{t_f} dt [a_{\text{out}}^\dagger(t) - a_{\text{out}}(t)], \quad (\text{D.1})$$

corresponding to the integrated homodyne-detection signal for measurement time  $t_f$ . In Eq. (D.1), we have introduced the output field  $a_{\text{out}}(t)$  leaking from a cavity with damping rate  $\kappa$ . The operator  $M$  is in turn used to define the measurement signal  $X$  and noise  $\Xi$ ,

$$X = |\langle M \rangle_+ - \langle M \rangle_-|, \quad (\text{D.2})$$

$$\Xi = (\Delta M_+^2 + \Delta M_-^2)^{1/2}, \quad (\text{D.3})$$

$$\Delta M_{\pm}^2 = \langle M^2 \rangle_{\pm} - \langle M \rangle_{\pm}^2, \quad (\text{D.4})$$

where  $\langle O \rangle_{\pm} \equiv \text{tr}[O(t_f)\rho_{\pm}(0)]$  and  $\rho_{\pm}(0) \equiv |\pm\rangle\langle\pm|_q \otimes |0\rangle\langle 0|_c$ , with  $|\pm\rangle_q$  the eigenstates of  $\sigma_x$  with eigenvalues  $\pm 1$ , respectively. The signal-to-noise ratio is then simply

$$\text{SNR} = X/\Xi. \quad (\text{D.5})$$



To evaluate the SNR for a given measurement scheme, it is useful to relate  $M$  to the input field  $a_{\text{in}}(t)$  and to the field  $a(t)$  inside the cavity. This relation is given by the input-output formula [47]

$$a_{\text{out}}(t) = a_{\text{in}}(t) + \sqrt{\kappa} a(t). \quad (\text{D.6})$$

Assuming that the input is vacuum, substitution of Eq. (D.6) into Eq. (D.1) gives

$$\langle M \rangle_{\pm} = i\kappa \int_0^{t_f} dt [\langle a^{\dagger}(t) \rangle_{\pm} - \langle a(t) \rangle_{\pm}], \quad (\text{D.7})$$

$$\langle M^2 \rangle_{\pm} = \kappa t_f + 2\kappa^2 \int_0^{t_f} dt_1 \int_0^{t_f-t_1} dt_2 [\langle a^{\dagger}(t_1+t_2)a(t_1) \rangle_{\pm} - \langle a(t_1+t_2)a(t_1) \rangle_{\pm} + \text{H.c.}]. \quad (\text{D.8})$$

Eqs. (D.7) and (D.8) relate  $\langle M \rangle_{\pm}$  and  $\langle M^2 \rangle_{\pm}$  – and thus the SNR – to simple expectation values and autocorrelation functions of the cavity field  $a(t)$ . Employing standard formulas [47], these expectation values and autocorrelation functions are easily calculated knowing the time-evolution operator  $V(t, t_0)$  of the qubit-cavity system. We find  $V(t, t_0)$  by solving the (time-inhomogeneous) master equation

$$\dot{V}(t, t_0) = \mathcal{L}(t)V(t, t_0). \quad (\text{D.9})$$

In Eq. (D.9), we have introduced the Lindbladian  $\mathcal{L}(t)$  describing cavity damping at rate  $\kappa$  and unitary evolution under the qubit-cavity toggling-frame Hamiltonian,  $H_{\text{T}}(t)$ ,

$$\mathcal{L}(t) \cdot = -i[H_{\text{T}}(t), \cdot] + \kappa \mathcal{D}[a] \cdot, \quad (\text{D.10})$$

$$\mathcal{D}[a] \cdot = a \cdot a^{\dagger} - \frac{1}{2} (a^{\dagger} a \cdot + \cdot a^{\dagger} a), \quad (\text{D.11})$$

where the centerdot (“ $\cdot$ ”) represents an arbitrary operator upon which the relevant superoperator is applied. In Eq. (D.10),  $H_{\text{T}}(t)$  is given by Eq. (4), taking  $\xi = 0$  and  $g(t) = g \forall t$ .

To evaluate  $V(t, t_0)$  analytically, we assume that  $t - t_0 = 2n_p\tau$ . We then use the Magnus expansion

$$V(t, t_0) = \exp \left[ \sum_{k=0}^{\infty} \bar{\mathcal{L}}^{(k)}(t - t_0) \right]. \quad (\text{D.12})$$

As in average Hamiltonian theory, the terms  $\bar{\mathcal{L}}^{(k)}$  are time-independent because  $\mathcal{L}(t)$  is periodic,  $\mathcal{L}(t + 2\tau) = \mathcal{L}(t) \forall t$ . Explicit expressions for  $\bar{\mathcal{L}}^{(k)}$  are given in the literature [37].

To gain insight into the problem, we evaluate the SNR to leading order in the Magnus expansion, Eq. (D.12). In this first approach, we neglect any qubit decay that may arise from higher-order terms in the expansion. We then find

$$V(t, t_0) = \exp[\bar{\mathcal{L}}^{(0)}(t - t_0)], \quad (\text{D.13})$$

$$\bar{\mathcal{L}}^{(0)} \cdot = -i[\bar{H}^{(0)}, \cdot] + \kappa \mathcal{D}[a] \cdot, \quad (\text{D.14})$$

$$\bar{H}^{(0)} = \frac{g}{2}(a + a^{\dagger})\sigma_x. \quad (\text{D.15})$$

According to Eqs. (D.13) and (D.14), the qubit forever remains in its initial state  $|\pm\rangle\langle\pm|_q$ . For  $\kappa t_f \gg 1$ , the cavity correspondingly settles in the coherent state  $|\alpha\rangle\langle\alpha|_c = |\mp ig/\kappa\rangle\langle\mp ig/\kappa|_c$ . Since the cavity field leaks from the output port at rate  $\kappa/2$ , this steady state leads to  $X \propto \kappa t_f \times g/\kappa \propto g t_f$ . In addition, noise in the output field then entirely comes from shot noise:  $\Delta M_{\pm}^2 = \kappa t_f$ , giving [42]

$$X = 4g t_f, \quad \Xi = \sqrt{2\kappa t_f} \Rightarrow \text{SNR} \propto \sqrt{t_f}. \quad (\text{D.16})$$

Therefore, in this ideal scenario, signal always accumulates faster than noise, making it possible to achieve arbitrarily large SNR simply by increasing  $t_f$ .

In practice, qubit relaxation leads to saturation of the signal and to enhancement of the noise, thus limiting the achievable SNR. Qubit relaxation can be intrinsic, coming from coupling of the qubit to a decay channel independent of the cavity. Higher-order corrections to the leading-order Magnus expansion taken here also lead to qubit decay via the cavity. This can be seen by means of a short-time expansion of  $\langle\sigma_x(t)\rangle_{\pm}$ . Indeed, the term of order  $\mathcal{O}(t)$  in this short-time expansion gives decay at a rate analogous to that of Purcell decay:

$$\Gamma \equiv \left| \frac{d}{dt} \langle\sigma_x(t)\rangle_{\pm} \right|_{t \rightarrow 0} \simeq |\text{tr}\{[\bar{\mathcal{L}}^{(2)\dagger} \sigma_x] \rho_{\pm}(0)\}| = \frac{g^2 \tau^2}{24} \kappa, \quad (\text{D.17})$$

where  $\rho_{\pm}(0) = |\pm\rangle\langle\pm|_q \otimes |0\rangle\langle 0|_c$ . The term of order  $\mathcal{O}(t)$  in the above expansion of  $\langle\sigma_x(t)\rangle_{\pm}$  dominates over the correction term of order  $\mathcal{O}(t^2)$  when  $\kappa t < 256/[3(\kappa\tau)^2]$ .

To take qubit relaxation into account in the calculation of the SNR, we employ the Langevin equation for the cavity field  $a(t)$ , considering the average Hamiltonian  $\bar{H}^{(0)}$  in Eq. (D.15). This gives

$$\dot{a}(t) + \frac{\kappa}{2} a(t) = -i \frac{g}{2} \sigma_x(t) - \sqrt{\kappa} a_{\text{in}}(t). \quad (\text{D.18})$$

Eq. (D.18) has the form of the equation of motion of a Brownian particle with mass  $m$ , momentum  $p$ , and friction coefficient  $\gamma$ :  $\dot{p} + (\gamma/m)p = \eta(t)$  [47]. In Eq. (D.18), the fluctuating force  $\eta(t)$  comes from a combination of shot noise from the input field  $a_{\text{in}}(t)$  and telegraph noise from the qubit through the Heisenberg-picture operator  $\sigma_x(t)$ . Assuming that qubit-cavity coupling is turned on at time  $t = 0$  and that the cavity interacts with its environment since  $t \rightarrow -\infty$ , the solution of Eq. (D.18) is

$$a(t) = -i \frac{g}{2} \int_0^t dt' e^{-\kappa(t-t')/2} \sigma_x(t') - \sqrt{\kappa} \int_{-\infty}^t dt' e^{-\kappa(t-t')/2} a_{\text{in}}(t'). \quad (\text{D.19})$$

For a qubit undergoing simultaneous excitation and relaxation at equal rates  $\Gamma/2$  in the eigenbasis of  $\sigma_x$ , we have

$$\langle\sigma_x(t)\rangle_{\pm} = \pm \exp(-\Gamma t), \quad (\text{D.20})$$

$$\langle\sigma_x(t)\sigma_x(t')\rangle_{\pm} = \exp(-\Gamma|t-t'|). \quad (\text{D.21})$$

Substituting Eqs. (D.19) to Eq. (D.21) into Eqs. (D.7) and (D.8), we evaluate the signal and noise using Eq. (D.2) and Eq. (D.3). We find

$$X = \frac{2g\kappa}{\kappa/2 - \Gamma} \left( \frac{1 - e^{-\Gamma t_f}}{\Gamma} - \frac{1 - e^{-\kappa t_f/2}}{\kappa/2} \right), \quad (\text{D.22})$$

$$\Xi = \sqrt{2\kappa t_f + \frac{4g^2\kappa^2}{(\kappa^2/4 - \Gamma^2)\Gamma^2} f(t_f) - \frac{X^2}{2}}, \quad (\text{D.23})$$

where we have introduced

$$\begin{aligned} f(t) = & \Gamma t - \frac{\Gamma}{\Gamma + \kappa/2} \left( 1 + \frac{2\Gamma}{\kappa} \right) \left[ 1 - e^{-(\Gamma + \kappa/2)t} \right] - \left( 1 - \frac{2\Gamma}{\kappa} e^{-\kappa t/2} \right) (1 - e^{-\Gamma t}) \\ & + \frac{2\Gamma}{\kappa} (1 - e^{-\kappa t/2}) \left[ e^{-\Gamma t} + \frac{\Gamma}{\kappa} (1 - e^{-\kappa t/2}) \right] - \frac{4\Gamma^2}{\kappa^2} \left[ \Gamma t - \frac{\Gamma}{\kappa} (3 - 4e^{-\kappa t/2} + e^{-\kappa t}) \right]. \end{aligned} \quad (\text{D.24})$$

To simplify the above expressions, we expand  $X$  and  $f(t)$  to leading order in  $\Gamma t_f$  around  $\Gamma t_f = 0$ . We also assume that the cavity has reached its steady state; we thus have  $\Gamma t_f \ll 1 \ll \kappa t_f$ . Therefore, in Eqs. (D.22) and (D.24), we drop exponentially small corrections in  $\kappa t_f \gg 1$ . In Eq. (D.22), we also drop terms of order  $\mathcal{O}(\Gamma/\kappa)$  or higher, which do not change the dependence of  $X$  and  $\Xi$  on  $t_f$ . However, in Eq. (D.24), we keep the terms of order  $\mathcal{O}(\Gamma/\kappa)$ , since they grow faster than linearly with  $t_f$ , but drop corrections of order  $\mathcal{O}(\Gamma^2/\kappa^2)$  or higher. We then find

$$X \simeq 4gt_f, \quad \Xi \simeq \sqrt{2\kappa t_f + \frac{16}{3}g^2\Gamma t_f^3}. \quad (\text{D.25})$$

Equation (D.25) shows that  $\Xi^2$  contains two terms: one from photon shot noise,  $\propto \kappa t_f$ , and an additional contribution from qubit switching,  $\propto g^2\Gamma t_f^3$ . Therefore, including qubit switching, the noise grows faster than the signal ( $\propto t_f$ ) as a function of  $t_f$ . This is visible in Fig. D1(a), in which we plot  $X(t_f)$  and  $\Xi(t_f)$  resulting from an exact numerical solution of the master equation given by Eq. (D.9). In Fig. D1(a),  $X(t_f)$  and  $\Xi(t_f)$  are represented by the solid black line and the dotted red line, respectively. Using the dashed blue line, we also plot  $\Xi(t_f) = \sqrt{2\kappa t_f}$ , expected for pure photon shot noise, Eq. (D.16). Clearly, excess noise due to qubit decay determines the measurement time  $t_{\text{opt}}$ , that maximizes the SNR [shown by the double arrow in Fig. D1(a)]. We evaluate  $t_{\text{opt}}$  analytically by maximizing  $\text{SNR} = X/\Xi$ , with  $X$  and  $\Xi$  given by Eq. (D.25). We find

$$\Gamma t_{\text{opt.}} \simeq \frac{1}{2} \sqrt{\frac{3}{2}} \frac{\sqrt{\kappa\Gamma}}{g}, \quad (\text{D.26})$$

$$\text{SNR} \simeq \left( \frac{6g^2}{\kappa\Gamma} \right)^{1/4}. \quad (t_f = t_{\text{opt.}}) \quad (\text{D.27})$$

Equation (D.27) provides a simple relationship between the maximal SNR and the cooperativity  $C \equiv g^2/\kappa\Gamma$ ,  $\text{SNR} \simeq (6C)^{1/4}$ .

Equation (D.27) gives the maximal SNR when the qubit undergoes switching in the eigenbasis of  $\sigma_x$ . As seen above, this can be due to the subleading term  $\bar{\mathcal{L}}^{(2)}$  in the Magnus expansion, Eq. (D.12), which leads the qubit to decay at the rate given in Eq. (D.17). When this mechanism is the dominant source of decay in the eigenbasis of  $\sigma_x$ , we substitute Eq. (D.17) into Eq. (D.27) to find the corresponding optimal SNR,

$$\text{SNR} \simeq \frac{2\sqrt{3}}{\sqrt{\kappa\tau}}, \quad (t_f = t_{\text{opt.}}) \quad (\text{D.28})$$

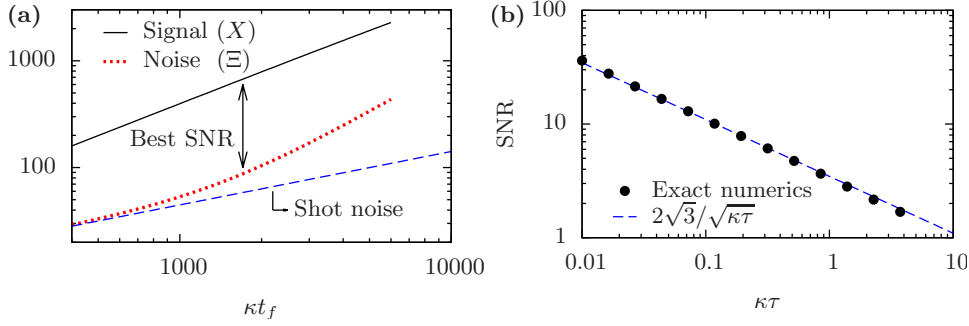


**Figure D1.** Signal-to-noise ratio (SNR) for the proposed readout with  $g/\kappa = 1/10$ . (a) Dynamics of signal and noise accumulation for measurement time  $t_f$ . Solid black line: measurement signal  $X$ , Eq. (D.2). Red dotted line: measurement noise  $\Xi$ , Eq. (D.3). Dashed blue line:  $\Xi$  for shot noise only, Eq. (D.16). The double arrow indicates the measurement time that optimizes the ratio  $\text{SNR} = X/\Xi$ .  $S$  and  $\Xi$  are evaluated for  $\kappa\tau = 0.2$ . (b) Maximal SNR as a function of  $\kappa\tau$ . In (a) and (b),  $X$  and  $\Xi$  are evaluated using a numerical solution of the master equation, Eq. (D.9). For  $g/\kappa = 1/10$ , a cavity Hilbert space of dimension 3 is sufficient for accurate numerical evaluation of  $X$  and  $\Xi$ .

valid for  $\Gamma t_f \ll 1 \ll \kappa t_f \ll 256/[3(\kappa\tau)^2]$ . The last inequality arises from the short-time expansion performed in Eq. (D.17). Equation (D.28) implies that  $\text{SNR} > 1$  is achievable even in the weak-coupling regime,  $g < \kappa$ . This result is shown in Fig. D1(b), in which we plot the maximal SNR obtained from an exact numerical solution of Eq. (D.9) as the black dots for  $g/\kappa = 1/10$ . This numerical result is in good agreement with the optimal SNR given in Eq. (D.28), displayed as the dashed blue line.

We now discuss conditions under which the dynamics of the proposed readout are accurately described by the Magnus expansion [Eq. (D.12)], up to and including order  $\bar{\mathcal{L}}^{(2)}$ . The Magnus expansion converges rapidly when  $\int_0^{2\tau} dt \|\mathcal{L}(t)\|_2 \ll 1$  [37]. For  $g < \kappa$ , the steady-state cavity population is small:  $\langle a^\dagger a(t) \rangle = (g/\kappa)^2 < 1$  for  $\kappa t_f \gg 1$ . In this situation, we can represent the operators  $a$  and  $a^\dagger$  by truncated matrices of small dimension, making  $\|a^{(\dagger)}\|_2 \sim 1$ . This implies that  $\|\mathcal{L}(t)\|_2 \sim \kappa$ , and we conclude that truncating the Magnus expansion is justified for  $\kappa\tau < 1$  under the assumption that  $g < \kappa$ . This statement is supported by Fig. D1(b), which shows excellent agreement between the exact numerical solution (represented by the black dots) and Eq. (D.28) (represented by the dashed blue line) for  $\kappa\tau < 1$ .

The SNR given in Eq. (D.28) is useful to describe the measurement of qubit expectation values through a soft average [48, 49]. However, to characterize single-shot readout, the full probability distribution of the measurement outcomes is needed. Indeed, qubit switching leads to a non-Gaussian probability distribution which is not fully characterized by its first two moments, given in Eq. (D.25). To evaluate the full probability distribution, we use a classical readout model that takes into account qubit switching at symmetric rates  $\Gamma/2$ , where  $\Gamma$  is given by Eq. (D.17) [51, 50]. This probability distribution leads to a single-shot fidelity that converges asymptotically to

$$F_1 = 1 - \frac{(\kappa\tau)^2}{192} \left[ \log \frac{96}{(\kappa\tau)^2} + \mathcal{O} \left( \log^{-1/2} \kappa\tau \right) \right] \quad (\text{D.29})$$

as  $\kappa\tau \rightarrow 0$ . Taking  $\kappa\tau = 0.1$  then leads to  $F_1 = 99.95\%$ , showing that the error due to the subleading term in the Magnus expansion is rapidly suppressed in the limit of short pulse intervals.

## References

- [1] Schuster D I, Sears A P, Ginossar E, DiCarlo L, Frunzio L, Morton J J L, Wu H, Briggs G A D, Buckley B B, Awschalom D D and Schoelkopf R J 2010 *Phys. Rev. Lett.* **105**(14) 140501
- [2] Amsüss R, Koller C, Nöbauer T, Putz S, Rotter S, Sandner K, Schneider S, Schramböck M, Steinhauser G, Ritsch H, Schmiedmayer J and Majer J 2011 *Phys. Rev. Lett.* **107**(6) 060502
- [3] Kubo Y, Grezes C, Dewes A, Umeda T, Isoya J, Sumiya H, Morishita N, Abe H, Onoda S, Ohshima T, Jacques V, Dréau A, Roch J F, Diniz I, Auffeves A, Vion D, Esteve D and Bertet P 2011 *Phys. Rev. Lett.* **107**(22) 220501
- [4] Petersson K D, McFaul L W, Schroer M D, Jung M, Taylor J M, Houck A A and Petta J R 2012 *Nature (London)* **490** 380–382
- [5] Viennot J J, Dartiaillh M C, Cottet A and Kontos T 2015 *Science* **349** 408
- [6] Beaudoin F, Lachance-Quirion D, Coish W A and Poro-Ladrière M 2016 *arXiv:1606.04736*
- [7] Haroche S and Raimond J M 2006 *Exploring the Quantum: Atoms, Cavities, and Photons* (Oxford, England: Oxford University Press)
- [8] Putz S, Angerer A, Krimer D O, Glattauer R, Munro W J, Rotter S, Schmiedmayer J and Majer J 2015 *arXiv:1512.00248*
- [9] Balasubramanian G, Neumann P, Twitchen D, Markham M, Kolesov R, Mizuochi N, Isoya J, Achard J, Beck J, Tissler J *et al.* 2009 *Nature mater.* **8** 383–387
- [10] Muhonen J T, Dehollain J P, Laucht A, Hudson F E, Sekiguchi T, Itoh K M, Jamieson D N, McCallum J C, Dzurak A S and Morello A 2014 *Nat. Nanotechnol.* **9** 986–991
- [11] Siyushev P, Xia K, Reuter R, Jamali M, Zhao N, Yang N, Duan C, Kukharchyk N, Wieck A D, Kolesov R *et al.* 2014 *Nat. Commun.* **5** 3895
- [12] Veldhorst M, Hwang J C C, Yang C H, Leenstra A W, de Ronde B, Dehollain J P, Muhonen J T, Hudson F E, Itoh K M, Morello A and Dzurak A S 2014 *Nat. Nanotechnol.* **9** 981–985
- [13] Bluhm H, Foletti S, Neder I, Rudner M, Mahalu D, Umansky V and Yacoby A 2010 *Nat. Phys.* **7** 109
- [14] Trif M, Golovach V N and Loss D 2008 *Phys. Rev. B* **77**(4) 045434
- [15] Hu X, Liu Y X and Nori F 2012 *Phys. Rev. B* **86**(3) 035314
- [16] Jin P Q, Marthaler M, Shnirman A and Schön G 2012 *Phys. Rev. Lett.* **108**(19) 190506
- [17] Kloeffer C, Trif M, Stano P and Loss D 2013 *Phys. Rev. B* **88**(24) 241405
- [18] Tosi G, Mohiyaddin F A, Tenberg S B, Rahman R, Klimeck G and Morello A *arXiv:1509.08538*
- [19] Dial O E, Shulman M D, Harvey S P, Bluhm H, Umansky V and Yacoby A 2013 *Phys. Rev. Lett.* **110**(14) 146804
- [20] Laird E A, Pei F and Kouwenhoven L P 2013 *Nat. Nanotechnol.* **8** 565–568
- [21] Wesenberg J H, Ardavan A, Briggs G A D, Morton J J L, Schoelkopf R J, Schuster D I and Mølmer K 2009 *Phys. Rev. Lett.* **103**(7) 070502
- [22] Kubo Y, Ong F R, Bertet P, Vion D, Jacques V, Zheng D, Dréau A, Roch J F, Auffeves A, Jelezko F *et al.* 2010 *Phys. Rev. Lett.* **105**(14) 140502
- [23] Kubo Y, Diniz I, Dewes A, Jacques V, Dréau A, Roch J F, Auffeves A, Vion D, Esteve D and Bertet P 2012 *Phys. Rev. A* **85**(1) 012333
- [24] Viola L, Knill E and Lloyd S 1999 *Phys. Rev. Lett.* **82**(12) 2417–2421
- [25] Khodjasteh K and Viola L 2009 *Phys. Rev. A* **80**(3) 032314
- [26] Khodjasteh K and Viola L 2009 *Phys. Rev. Lett.* **102**(8) 080501
- [27] West J R, Lidar D A, Fong B H and Gyure M F 2010 *Phys. Rev. Lett.* **105**(23) 230503
- [28] Jobez P, Laplane C, Timoney N, Gisin N, Ferrier A, Goldner P and Afzelius M 2015 *Phys. Rev. Lett.* **114**(23) 230502
- [29] Saglamyurek E, Jin J, Verma V B, Shaw M D, Marsili F, Nam S W, Oblak D and Tittel W 2015 *Nature Photonics* **9** 83–87
- [30] Diniz I, Portolan S, Ferreira R, Gérard J M, Bertet P and Auffèves A 2011 *Phys. Rev. A* **84**(6) 063810
- [31] Kurucz Z, Wesenberg J H and Mølmer K 2011 *Phys. Rev. A* **83**(5) 053852
- [32] Cottet A and Kontos T 2010 *Phys. Rev. Lett.* **105**(16) 160502
- [33] Gambetta J M, Houck A A and Blais A 2011 *Phys. Rev. Lett.* **106**(3) 030502
- [34] Srinivasan S J, Hoffman A J, Gambetta J M and Houck A A 2011 *Phys. Rev. Lett.* **106**(8) 083601

- [35] Mehring M 1976 *High Resolution NMR in Solids* (Springer)
- [36] Haeberlen U and Waugh J S 1968 *Phys. Rev.* **175**(2) 453–467
- [37] Blanes S, Casas F, Oteo J and Ros J 2009 *Phys. Rep.* **470** 151 ISSN 0370-1573
- [38] Yoneda J, Otsuka T, Nakajima T, Takakura T, Obata T, Pioro-Ladrière M, Lu H, Palmstrøm C J, Gossard A C and Tarucha S 2014 *Phys. Rev. Lett.* **113**(26) 267601
- [39] Coish W A and Loss D 2007 *Phys. Rev. B* **75**(16) 161302
- [40] Chesi S, Wang Y D, Yoneda J, Otsuka T, Tarucha S and Loss D 2014 *Phys. Rev. B* **90** 235311
- [41] Tosi G, Mohiyaddin F A, Huebl H and Morello A 2014 *AIP Adv.* **4** 087122
- [42] Didier N, Bourassa J and Blais A 2015 *Phys. Rev. Lett.* **115**(20) 203601
- [43] Scully M O and Zubairy M S 1997 *Quantum Optics* (Cambridge University Press)
- [44] Leghtas Z, Kirchmair G, Vlastakis B, Devoret M H, Schoelkopf R J and Mirrahimi M 2013 *Phys. Rev. A* **87**(4) 042315
- [45] Vlastakis B, Kirchmair G, Leghtas Z, Nigg S E, Frunzio L, Girvin S M, Mirrahimi M, Devoret M H and Schoelkopf R J 2013 *Science* **342** 607–610
- [46] Wang L, Tu T, Gong B and Guo G C 2015 *Phys. Rev. A* **92**(6) 062346
- [47] Gardiner C W and Zoller P 2000 *Quantum Noise* (Berlin: Springer)
- [48] D’Anjou B and Coish W A 2014 *Phys. Rev. Lett.* **113** 230402
- [49] Ryan C A, Johnson B R, Gambetta J M, Chow J M, da Silva M P, Dial O E and Ohki T A 2015 *Phys. Rev. A* **91** 022118
- [50] D’Anjou B and Coish W A 2014 *Phys. Rev. A* **89**(1) 012313
- [51] Gambetta J, Braff W A, Wallraff A, Girvin S M and Schoelkopf R J 2007 *Phys. Rev. A* **76**(1) 012325
- [52] Frey T, Leek P J, Beck M, Blais A, Ihn T, Ensslin K and Wallraff A 2012 *Phys. Rev. Lett.* **108**(4) 046807
- [53] Basset J, Stockklauser A, Jarausch D D, Frey T, Reichl C, Wegscheider W, Wallraff A, Ensslin K and Ihn T 2014 *Appl. Phys. Lett.* **105** 063105
- [54] Tabuchi Y, Ishino S, Noguchi A, Ishikawa T, Yamazaki R, Usami K and Nakamura Y 2015 *Science* **349** 405–408
- [55] Bylander J, Gustavsson S, Yan F, Yoshihara F, Harrabi K, Fitch G, Cory D, Nakamura Y, Tsai J S and Oliver W D 2011 *Nat. Phys.* **7** 565–570